Average solar wind and geomagnetic activity influence on the equatorial plasma mass density at geosynchronous orbit

V. Veibell and R.S. Weigel

July 28, 2016

Abstract

We consider two types of events, identified by decreases in D_{st} below a threshold value and increases in the the equatorial mass density at geosynchronous altitudes, ρ_{eq}, above a threshold value on 1-hour and 1-day time scales using the *Takahashi et al.* [2010] dataset. From the D_{st} events, we find that there is a weak and small amplitude ($< 10\%$) difference between ρ_{eq} on the day of the event and the days before and after on both daily and hourly timescales. Although very large geomagnetic storms have been observed to correspond to large increases in ρ_{eq}, on average, ρ_{eq} following the onset of a geomagnetic storm does not depend on the north-south component of the interplanetary magnetic field, B_z near onset time. From the ρ_{eq} events, we find a weak dependence on B_z after the onset of an event, with higher average B_z four hours after the event onset corresponding to larger ρ_{eq} events. In contrast, the average of B_z four hours prior to ρ_{eq} events does not have a statistically significant impact on ρ_{eq} after onset.

1   Introduction

The dependence of the plasmapause location on geomagnetic activity was observed as early as *Carpenter* [1966] and there are well–validated models of the plasmapause location as a function of L, MLT, and geomagnetic activity (*Lemaire* [1998], *Moldwin et al.* [2002], *O'Brien and Moldwin* [2003]). Models also exist for the plasmasphere density (*Gallagher et al.* [1988]; *Lemaire* [1998]) with similar parameterization.

The dependence of the plasma density outside of the nominal plasmapause location on geomagnetic and solar wind conditions has not been extensively studied until the past decade (*Takahashi et al.* [2006]; *Takahashi et al.* [2010]; *Denton et al.* [2016]). Earlier works that considered profiles of ion density found a significant dependence of the plasmapause location on geomagnetic activity (*Chappell et al.* [1970]; *Maynard and Grebowsky* [1977]; *Carpenter and Anderson* [1992]), but the relationship between geomagnetic activity and density outside of the plasmapause was not explicitly considered.

Takahashi et al. [2006] estimated magnetospheric mass density using measurements from the CRRES satellite during a 73-day period in 1991 when CRRES was in an elliptical, near equatorial orbit and primarily beyond the nominal plasmapause. They found that the local average ion mass, M, had some correlation with geomagnetic activity, with more negative hourly D_{st} values corresponding to higher M and 1.5- and 3-day averages of K_p corresponding to higher M (3-hour averages of K_p had little visual correlation with M). The mass density estimates were obtained from CRRES observations in the MLT range of [12:00, 18:00] with most observations at L between 5 and 7 R_E.

Denton et al. [2006] found a weak relationship between D_{st} and and K_p and the field line distribution of plasma mass density, ρ, using observations of the first three toroidal Alfvén harmonic frequencies for L in the range of 6-8 R_E. A more pronounced peak in the distribution along a field line near the equator was found for lower D_{st} and larger K_p, but the equatorial value of ρ was found to be similar for D_{st} bins of [-142, -31] and [-31, 37] nT and K_p bins of [1.5,3.4] and [3.4, 5.9].

47   *Takahashi et al.* [2010] developed a mass density dataset using measurements from the

48   Space Environment Monitor instruments on the Geostationary Operational Environmental

49   Satellites (GOES) satellites from 1980 through 1992, with most measurements in the range

50   of $L = 6.8 \pm 0.2 R_E$. The mass density was estimated using the the Alfvén wave velocity

51   relationship, $V_A = B/\sqrt{\mu_0 \rho}$, a magnetic field model, and a numerical solution to a wave

52   equation with an ionospheric boundary and the assumption of a zero resistance ionosphere.

53   The equatorial mass density, ρ_{eq}, was derived from the estimated mass density using a

54   power law dependence on the geocentric distance to the field line of the observation, R,

55    $\rho = \rho_{eq}(LR_E/R)^{1/2}$. They found a high correlation (~ 0.94) between 27-day averages of

56    $F10.7$ and 27-day medians of ρ_{eq}.

57   *Takahashi et al.* [2010] noted that downward drops in the D_{st} index coincided with sig-

58   nificant changes in ρ_{eq} for L near 6.8 R_E. For five storms, two had ρ_{eq} spikes after D_{st}

59   minimum, two had ρ_{eq} spikes before the drop, and one showed little change in ρ_{eq}. A key

60   result was that when daily-averaged measurements were considered, the epoch average of

61   D_{st} exhibited for storms with a minimum $D_{st} < -50$ nT showed an enhancement in ρ_{eq} the

62   same day as minimum D_{st} in the epoch averages.

63   *Yao et al.* [2008] studied the relationship between D_{st} and the number density of low-

64   energy O^+ in different regions (ring current and plasma sheet) using the TEAMS and ESA

65   instruments on the low-altitude and high-inclination orbiting FAST satellite and found that

66   the average N_{O+} across the sampled L-shells (2-14) had a strong correlation (0.88) with the

67   minimum D_{st} of the storm. Although the correlation at geosynchronous distances was not

68   calculated, the data presented for four events show that the enhancements in N_{O+} tended

69   to appear near D_{st} minimum ($\pm$ 2 hours).

70   The above results indicate that (1) the mass density in the at geosynchronous distances

71   is best correlated with $F10.7$ and (2) there exists a much weaker statistical relationship

72   between mass density and the geomagnetic activity indices K_p and D_{st}. In this work we

73   consider the dependence of mass density estimates in the *Takahashi et al.* [2010] data set

74 and attempt to identify and statistically characterize the relationship between geomagnetic

75 activity with mass density at geosynchronous distances. In addition, we attempt to identify

76 solar wind processes that may drive the changes.

77 2   Data Preparation and Overview

78 The parameters ρ_{eq} and $F_{10.7}$ are from the dataset of *Takahashi et al.* [2010]; data are

79 available from 1980 through 1991 from GOES 2, 3, 5, 6 and 7. All other parameters used

80 are from *Kondrashov et al.* [2014], which has coverage from 1972 through 2013 and are on

81 a 1–hour time grid. ρ_{eq} is the inferred equatorial mass density based on the 3rd harmonic

82 torodial frequency of magnetic field measurements as described in *Takahashi et al.* [2010].

83 The smallest cadence for ρ_{eq} values is 10 minutes. To compute an hourly median over the

84 same interval for which the solar wind parameters were averaged, the median of all ρ_{eq} values

85 in a given hour window was used. GOES 6 had the longest span of available data and the

86 primary results presented are for GOES 6 while measurements from other satellites were

87 used for consistency checks.

88   The top panel of Figure 2 shows the long-term trends of $\log_{10}(\rho_{eq})$ from GOES 6 and

89 $F_{10.7}$ computed using the median values in 27-day non-overlapping windows. A scatter plot

90 of these two lines is shown in the lower panel of Figure 2 along with that for 1–day and

91 1–hour medians. The linear correlation for GOES 6 using all measurements is found to

92 be 0.94, which is the same value documented by *Takahashi et al.* [2010] who used combined

93 measurements from all satellites in the time interval of 1980 through 1991 using the constraint

94 $0600 \leq MLT \leq 1200$, $K_{p3d} \geq 1.0$ and $D_{st} \geq -50$ nT. Our 27-day correlations for GOES

95 2, 5, and 7 are 0.81, 0.78, and 0.87, and the time range of coverage of measurements from

96 these satellites is 1980-01-01/1983-05-16, 1983-01-01/1987-02-28, and 1983-05-27/1991-08-

97 29, respectively.

3   Results

Two types of events are considered. The first is a drop in the D_{st} index below the threshold of -50 nT. These types of events are considered in order to determine if there is a well-defined ρ_{eq} dependence on geomagnetic activity/storms as indicated by the D_{st} index. It is expected that the plasmasphere will exhibit two responses near these threshold crossings. First is the movement of the plasmapause earthward (*Lemaire* [1998]) and the second is a possible change in density due to magnetospheric processes.

The second type of event is an increase in ρ_{eq} above a threshold of 20 amu/cm^3. It is expected that these increases will typically occur after period of quiet geomagnetic activity but may also be the result of increases in solar wind driven geomagnetic activity. In this case, the plasmapause boundary may move outward past geosynchronous orbit and the increase will be due to measurements being made inside the plasmapause. A second possible reason for the increase could be due to magnetospheric processes.

3.1 D_{st} Events

Our first analysis uses GOES-6 data only from the time interval 1989-1991, which corresponds with the interval used in the epoch analysis of *Takahashi et al.* [2010]. In this interval, there were 75 D_{st} events where D_{st} remained below the -50 nT threshold for at least 12 hours. For both types of events, the first hour of a local minimum D_{st} following a threshold crossing defines the zero epoch time, and for each event, $4 \cdot 24$ hours were considered before and $8 \cdot 24$ hours after event onset. For multiple detected threshold crossings within 24 hours of each other, the first crossing was selected as the event since visual inspection showed the following crossings to typically be from brief deviations during the recovery period. To compute the epoch averages on a daily time scale, the median value of all available measurements for all events centered on a window of ± 12 hours of the epoch zero hour was computed, and these averaging windows were shifted in increments of 24 hours. Similar results are obtained if we

123 first reduce each event time series to have a 1-day cadence by computing medians for each

124 event in 1-day bins and then compute the medians across events on each epoch day.

125   The stack plot in the upper panel of Figure 3 shows the epoch averages for the 75

126 events from 1989-1991. The minimum D_{st} median is -75 nT. Consistent with *Takahashi*

127 *et al.* [2010], D_{st} events correspond to elevated ρ_{eq} before and after the event, although the

128 magnitude of increase observed here is, on average, 4.5 amu/cm^3 (from $\sim$19 to $\sim$24 amu/cm^3)

129 instead of the increase of $\sim$10 amu/cm^3 found in Figure 11 of *Takahashi et al.* [2010]. The

130 vertical green bars in the ρ_{eq} plot show the number of ρ_{eq} values that were used to compute

131 the medians and red error lines. Error lines for each parameter are the standard deviation

132 of the values used in computing the median divided by the square root of the number of

133 values. For the non-ρ_{eq} parameters, the number of measurements used in computing the

134 medians is typically equal to the number of events, which is much larger than the number

135 of ρ_{eq} values as all available measurements were used instead of restricting to only values

136 where a ρ_{eq} value also existed.

137   In the lower panel of Figure 3, it is shown that the trends seen in the analysis of 1989-1991

138 also hold for the entire span of measurements from GOES 6 - a small elevation on the day

139 of the event relative to the day before and day after, with median averages after the day of

140 the event being slightly lower than that before.

141   To determine if the magnitude of the density medians in the top panel of Figure 3 on

142 epoch days -1, 0, and 1 are statistically different from each other, we used a two-population

143 bootstrap test. A bootstrap sample of the medians for each epoch day was created by

144 sampling the values used to compute the median on each epoch day with replacement. The

145 observed difference between the medians is shown in Table 1 along with the fraction of

146 observations in 1000 bootstrap differences with a different sign than that observed.

147   If a statistically significant difference in the medians between two days existed, the frac-

148 tion of bootstrap samples with a different sign is expected to be much smaller ($< 5\%$). In

149 terms of a hypothesis test, we cannot reject the null hypothesis that the medians are the

Days	Difference (amu/cm^3)	%
-1 0	-4.48	13.90% ≥ 0
-1 1	-1.46	32.60% ≥ 0
1 0	-3.02	20.70% ≥ 0

Table 1: Results of test on of means of ρ_{eq} shown in the top panel of Figure 3 between days of threshold crossing near (day = 1 or -1) or on the day of a D_{st} event (day = 0).

same with a confidence higher than 100 minus the % value shown in the table; the highest confidence level of 89% is in the difference between day 0 and day -1.

These tests indicate that there is not a statistically significant difference in medians of ρ_{eq} on the day before and day after a threshold crossing in D_{st}. In addition, the observed differences are on the order of only 20% of the value of ρ_{eq} on the onset day, which is similar to the variation in the observations over the displayed epoch time interval.

We have also considered hourly averages as shown in the top panel of Figure 4. A total of 333 D_{st} events were found in the interval of May 1983 through August 1991 with an average duration of 10 hours and a median duration of 3 hours. In this plot, the overall trend is similar to that found in the bottom panel of Figure 4 - ρ_{eq} is slightly elevated at the time of the threshold crossing of D_{st} with respect to the values one day before and after, but the elevation is small relative to the error bars around the time of the event onset.

The bottom panel of Figure 4 contains the events shown in the top panel under the constraint that D_{st} remained below -50 nT for at least twelve hours after the event onset time. In the time period of elevated mass density within 12 hours of the start of the event, there are only $\sim$4 samples per hourly interval. This result is consistent with previous observations of large mass density increases in the plasma trough region during large geomagnetic storms (*Yao et al.* [2008]; *Takahashi et al.* [2010]).

The top panel of Figure 4 shows that, on average, near the onset of D_{st} events there is not a significant reponse in ρ_{eq} while the bottom panel shows that for rare and large D_{st} events elevated ρ_{eq} can be observed. To determine if there is an IMF B_z dependence, the epoch curves in the top panel of Figure 4 for ρ_{eq} and B_z were separated into two parts depending

172 whether B_z was above or below its average four hours before and including the onset hour

173 and four hours after and including the hour of onset; the result is shown in Figure 5. Any

174 statistically significant difference at a 95% confidence level between the two parts is indicated

175 by a green dot on the horizontal axis using the same bootstrap method described previously.

176 (At this confidence level, false positives are expected to randomly occur 5% of the time, or

177 3.6 times for 72 values.) These two curves indicate that there is not a statistically significant

178 dependence on IMF B_z around the time of the onset of a D_{st} event.

179   The process for creating Figure 5 was repeated except using the sort variable $F10.7$

180 instead of B_z, as shown in Figure 6. As expected, difference between the epoch curves is

181 statistically significant at all times, as expected, but elevated $F10.7$ is associated with a peak

182 in the ρ_{eq} curve approximately 5 hours after onset. The values contributing to the peak were

183 compared to a baseline of all values 16-48 hours after onset via a Wilcoxon rank-sum test

184 and found to have significantly different medians at the 99% significance level.

3.2 ρ_{eq} Events
185

186 An alternative type of event can be defined that corresponds to large increases in ρ_{eq}. Figure 7

187 shows the epoch time series for events in which an increase of ρ_{eq} above 20 amu/cm^2 defines

188 the start of the event. In finding ρ_{eq} events, missing values were replaced with linearly

189 interpolated values. These events are associated with positive B_z and low values of D_{st}.

190 Approximately 8 hours after onset, ρ_{eq} peaks and then slowly decays after 40 hours to pre–

191 onset levels.

192   Figure 7 can be compared with Figure 9 of *Denton et al.* [2016], which shows daily

193 averages of ρ_{eq} from this dataset after the onset of quiet K_p intervals. The growth shown here

194 is approximately linear and lasts $\sim$ 12–18 hours whereas the 10 quiet K_p events considered

195 by *Denton et al.* [2016] showed growth that lasted for at least 48 hours.

196   The largest difference occurs when the separation is performed after onset, with more

197 positive B_z leading to larger peak ρ_{eq} than more negative B_z. The rate of change of ρ_{eq} also

198 appears to be insenstive to B_z for approximately 12 hours prior to onset. The equivalent

199 epoch separation curves for P_{dyn} had a statistically significant differences similar to that for

200 B_z, with higher dynamic pressure playing a role similar to positive B_z.

201 Figure 9 shows how the epoch average curve of ρ_{eq} in Figure 8 depends on $F10.7$. Sta-

202 tistically significant differences occur independent of if the separating factor the average of

203 $F10.7$ before or after onset, as expected because the cadence of $F10.7$ is one day and its

204 time scale of variation is longer than that of ρ_{eq}. Events with high $F10.7$ are associated with

205 higher ρ_{eq} before and after event onset but similar peak values. As was the case for B_Z,

206 there is an approximately 12–hour time span of linear growth of ρ_{eq} near the time of onset

207 but because the initial starting ρ_{eq} is higher for high $F10.7$, the associated growth rate is

208 lower.

209 ## 3.3   Summary and Conclusions

210 In recent years, various works have considered the influence of solar wind control and the

211 geomagnetic activity relationship to the equatorial plasma mass density at geosynchronous

212 orbit, generally using event studies and linear correlations (*Takahashi et al.* [2006]; *Denton*

213 *et al.* [2006]; *Yao et al.* [2008]; *Takahashi et al.* [2010]; *Denton et al.* [2016]). The event

214 studies show a possible relationship between ρ_{eq} and solar wind and geomagnetic activity

215 indicators such as K_p and D_{st} while correlation studies have generally found a very weak

216 relationship.

217 This work presents an analysis of two types of events intended to provide insight into the

218 relationship between ρ_{eq} and solar wind and geomagnetic parameters by considering both

219 large geomagnetic events and large ρ_{eq} events. The analysis attempts to address a major

220 difficulty with the identification of the cause in ρ_{eq} enhancements, which can occur for two

221 reasons: (1) an extended period of positive B_z, which leads to low geomagnetic activity,

222 plasmasphere refilling, and a possible expansion of the plasmasphere to geosynchronous

223 altitudes and (2) strong negative B_z, which (a) leads to the inward motion of the higher

224 density plasmasphere and leaves geosynchronous altitudes in the lower density plasma trough

225 just outside of the plasmapause and (b) causes possible magnetospheric processes to enhance

226 the mass density at geosynchronous altitudes.

227   On average, around the time of large geomagnetic events, there is a very weak enhance-

228 ment of ρ_{eq} and this enhancement does not depend on either the interplanetary magnetic

229 field B_z or the intensity of the geomagnetic event. This indicates that there is an approx-

230 imate balance between magnetospheric enhancement in ρ_{eq} and any reduction due to the

231 inward motion of the plasmasphere.

232   ρ_{eq} events are larger when B_z is more positive after the onset of the event, which indicates

233 that a substantial portion of the events may due to the apparent mass refilling mechanism

234 described by *Denton et al.* [2016]. Without additional information about the location of the

235 plasmapause, it may not be possible to separate out the conditions required for enhancement

236 due to enhanced magnetospheric activity from this mechanism.

References

Carpenter, D. L., Whistler studies of the plasmapause in the magnetosphere: 1. Temporal variations in the position of the knee and some evidence on plasma motions near the knee, *J. Geophys. Res.*, *71*, 693–709, 1966.

Carpenter, D. L., and R. R. Anderson, An ISEE/whistler model of equatorial electron density in the magnetosphere, *J. Geophys. Res.*, *97*, 1097–1108, 1992.

Chappell, C. R., K. K. Harris, and G. W. Sharp, A study of the influence of magnetic activity on the location of the plasmapause as measured by OGO 5, *J. Geophys. Res.*, *75*, 50–56, 1970.

Denton, R., Database of Input Parameters for Tsyganenko Magnetic Field Models, 2007.

Denton, R. E., K. Takahashi, I. A. Galkin, P. A. Nsumei, X. Huang, B. W. Reinisch, R. R. Anderson, M. K. Sleeper, and W. J. Hughes, Distribution of density along magnetospheric field lines, *J. of Geophys. Res.*, *111*, 4213, 2006.

Denton, R. E., K. Takahashi, J. Amoh, and H. J. Singer, Mass density at geostationary orbit and apparent mass refilling, *J. Geophys. Res.*, *121*, 2962–2975, 2016.

Gallagher, D. L., P. D. Craven, and R. H. Comfort, An empirical model of the earth's plasmasphere, *Advances in Space Research*, *8*, 15–21, 1988.

Kondrashov, D., R. Denton, Y. Y. Shprits, and H. J. Singer, Reconstruction of gaps in the past history of solar wind parameters, *Geophys. Res. Lett.*, *41*, 2702–2707, 2014.

Lemaire, J., *The Earth's Plasmasphere*, Cambridge University Press, 1998.

Maynard, N. C., and J. M. Grebowsky, The plasmapause revisited, *J. Geophys. Res.*, *82*, 1591–1600, 1977.

259 Moldwin, M. B., L. Downward, H. K. Rassoul, R. Amin, and R. R. Anderson, A new model

260   of the location of the plasmapause: CRRES results, *J. of Geophys. Res.*, *107*, 1339, 2002.

261 O'Brien, T. P., and M. B. Moldwin, Empirical plasmapause models from magnetic indices,

262   *Geophys. Res. Lett.*, *30*, 1–1, 2003.

263 Takahashi, K., R. E. Denton, R. R. Anderson, and W. J. Hughes, Mass density inferred from

264   toroidal wave frequencies and its comparison to electron density, *J. of Geophys. Res.*, *111*,

265   1201, 2006.

266 Takahashi, K., R. E. Denton, and H. J. Singer, Solar cycle variation of geosynchronous

267   plasma mass density derived from the frequency of standing Alfvén waves, *J. of Geophys.*

268   *Res.*, *115*, 7207, 2010.

269 Yao, Y., K. Seki, Y. Miyoshi, J. P. McFadden, E. J. Lund, and C. W. Carlson, Effect of solar

270   wind variation on low-energy O^+ populations in the magnetosphere during geomagnetic

271   storms: FAST observations, *J. of Geophys. Res.*, *113*, 2008.

272 4 Figures
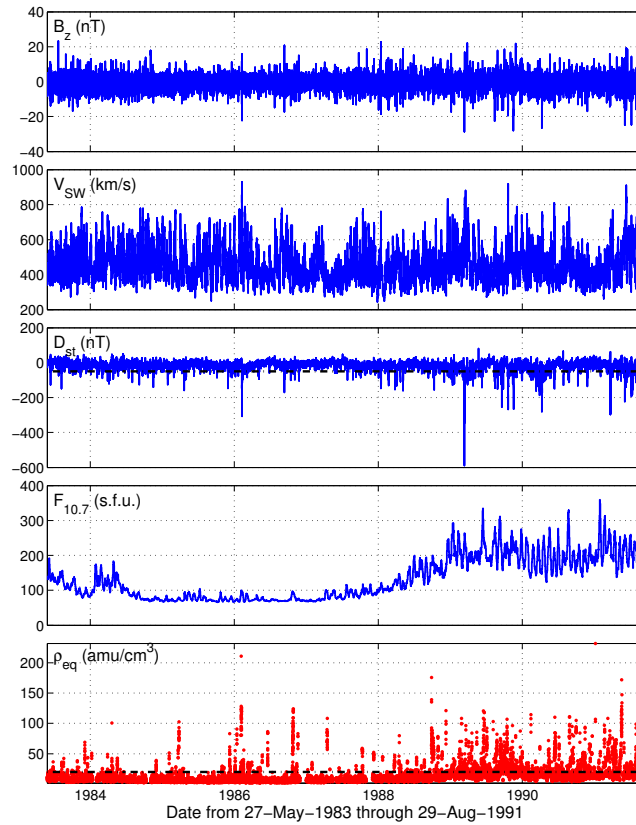
Figure 1: Overview of data used in this article. The top four panels show parameters from *Kondrashov et al.* [2014] and the bottom panel contains ρ_{eq} based on GOES 6 measurements from *Denton* [2007] after interpolation and averaging described in the text. Dashed horizontal lines in the D_{st} and ρ_{eq} panels indicate sample event cutoff thresholds of $D_{st} = -50$ nT and $\rho_{eq} = 20$ amu/cm^3 considered in Section 3.
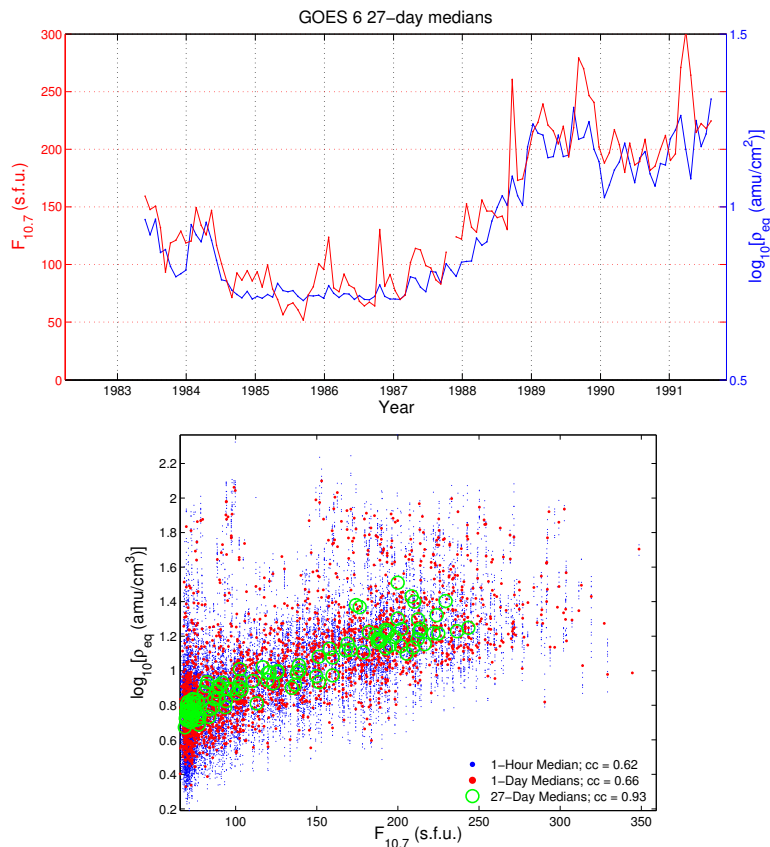
Figure 2: Top: 27-day non-overlapping medians of $F_{10.7}$ and $log(\rho_{eq})$ from GOES 6. Bottom: Correlation between $log(\rho_{eq})$ and $F_{10.7}$ using medians in non-overlapping hour, day, and 27-day windows.
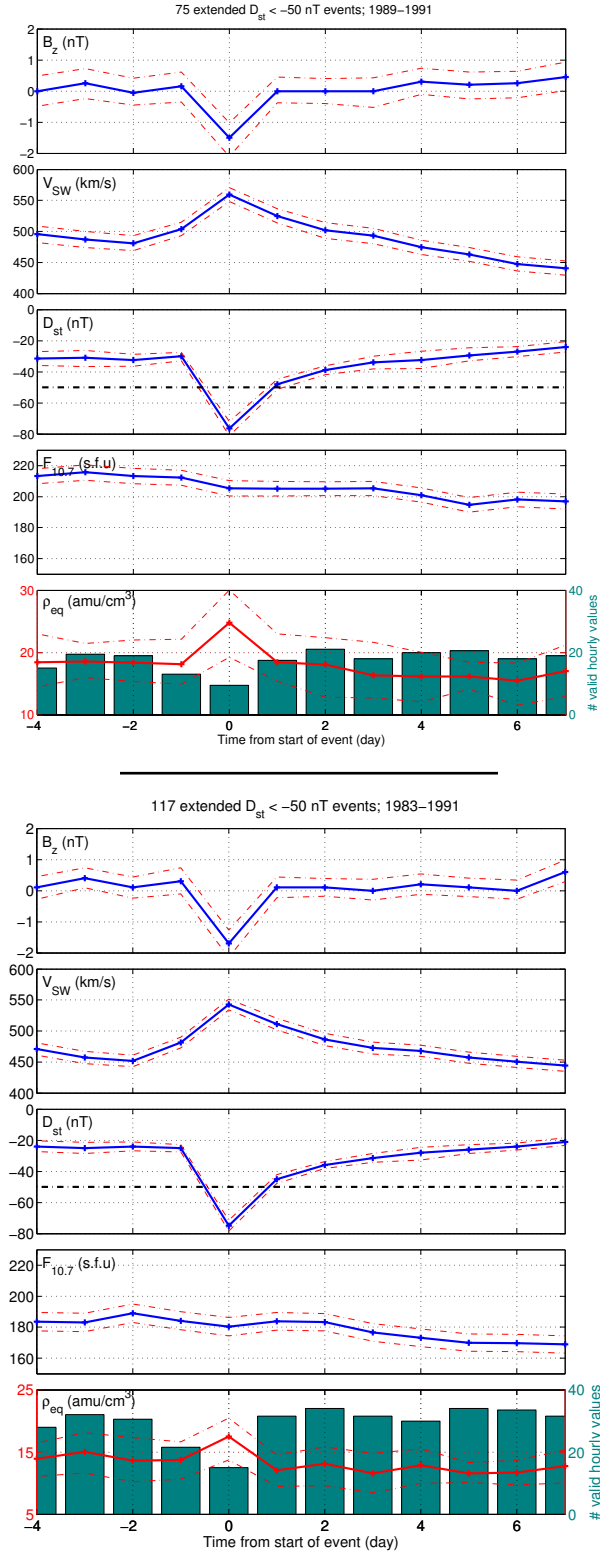
Figure 3: D_{st} events from GOES 6 using daily medians. Top: Events in the interval 1989-1991; compare to *Takahashi et al.* [2010] Figure 11. Bottom: Events in the interval 1983-1991.
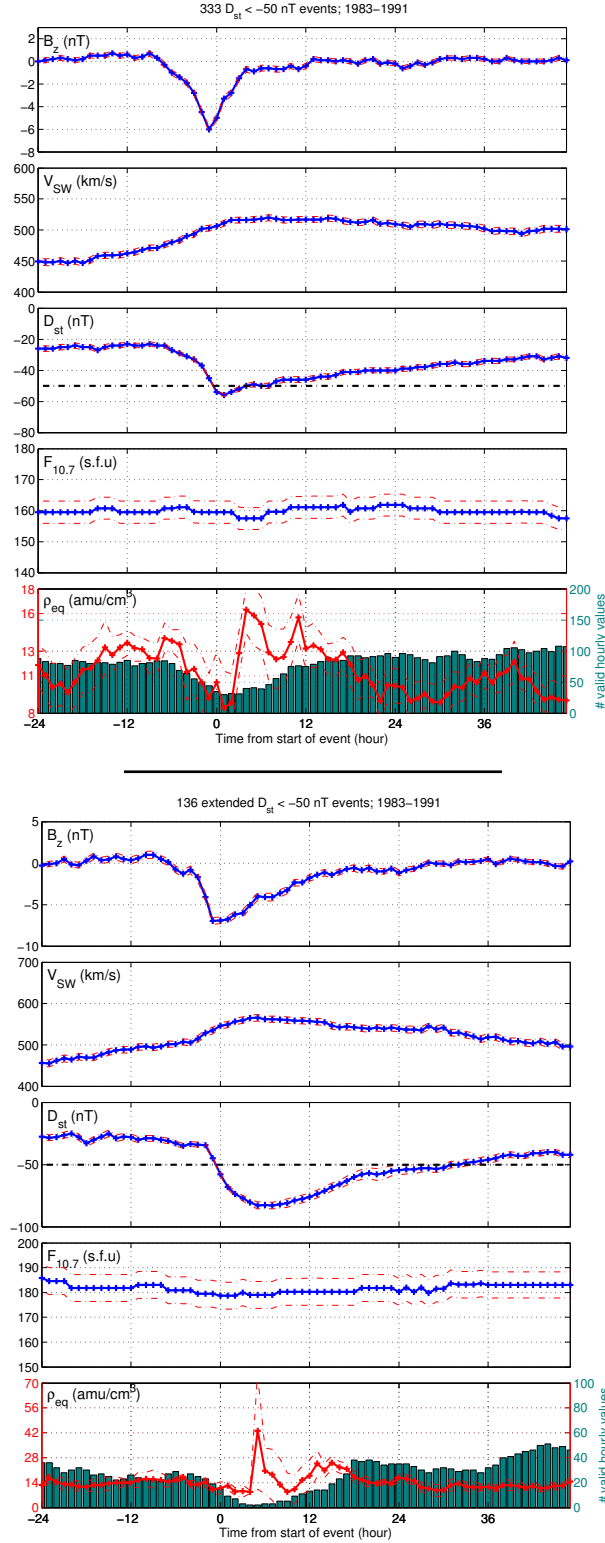
Figure 4: D_{st} events from GOES 6 using hourly medians. Top: Events in the interval 1983-1991. Bottom: Same as Top except for constraint that D_{st} stayed below -50 nT for at least 12 hours after crossing below -50 nT.
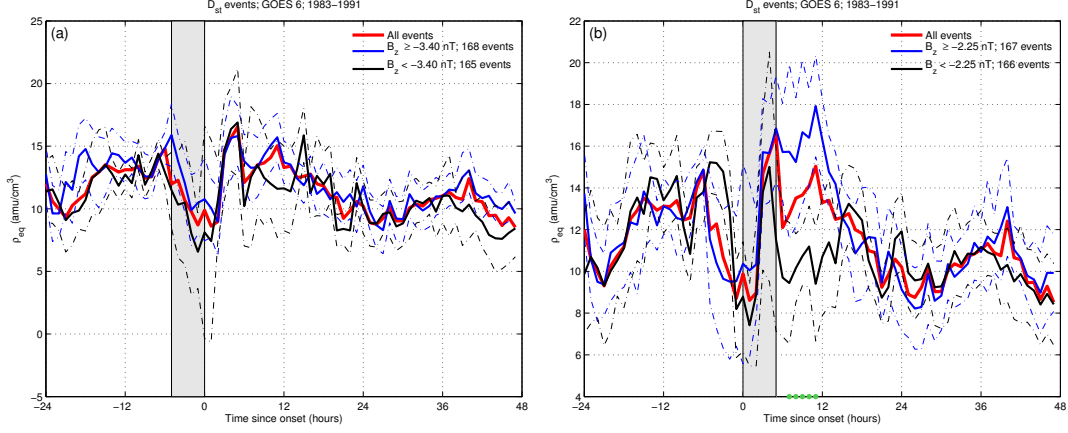
Figure 5: D_{st} events of Figure 4 separated by the average D_{st} value (a) at onset and four hours before, and (b) at onset and four hours after.
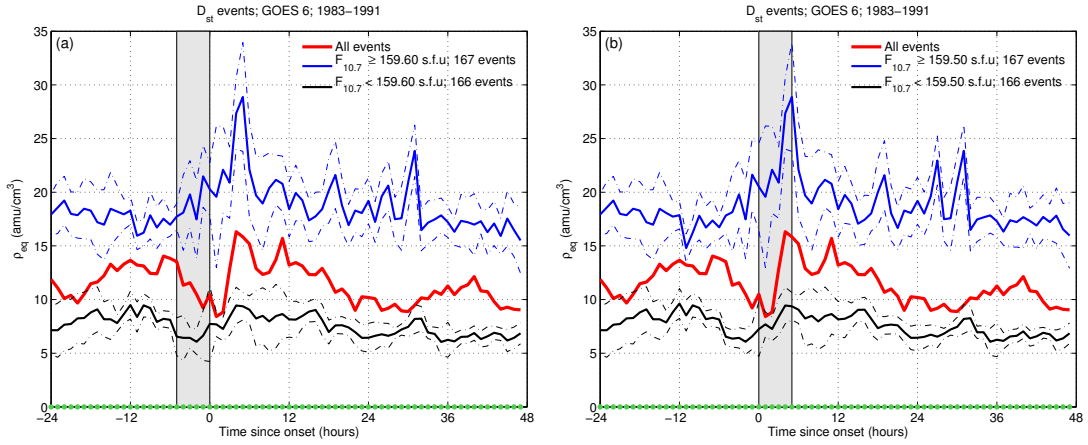
Figure 6: D_{st} events of Figure 4 separated by the average $F10.7$ value (a) at onset and four hours before, and (b) at onset and four hours after.
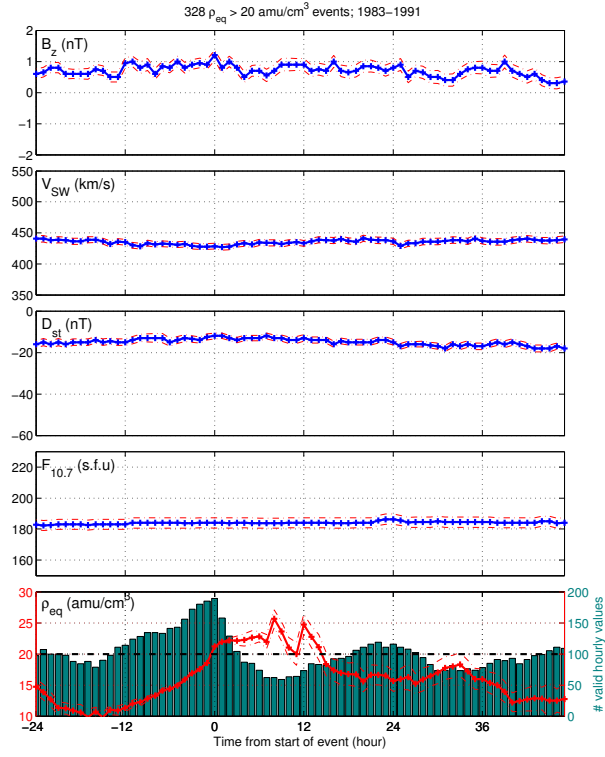
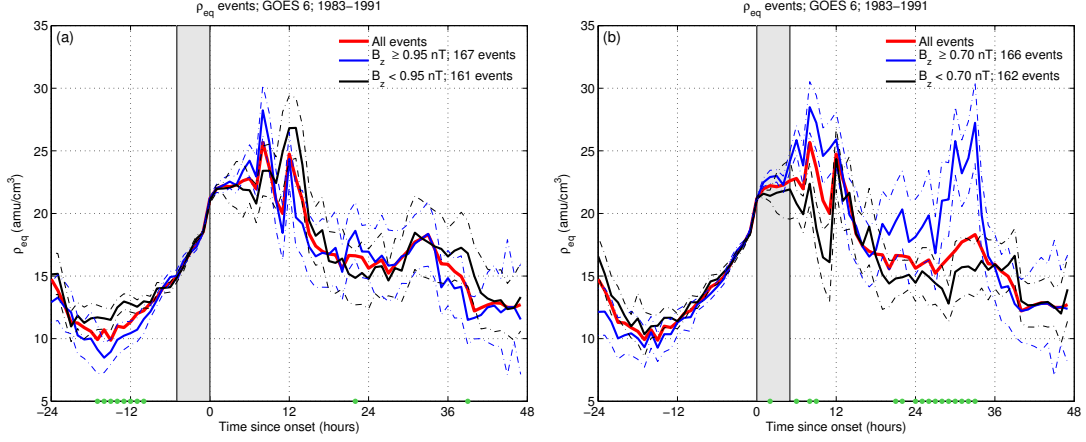Figure 7: $\rho_{eq} > 20$ amu/cm^3 events from GOES 6 using hourly medians.

Figure 8: ρ_{eq} events of Figure 7 separated by the average B_z value (a) at onset and four hours before, and (b) at onset and four hours after.
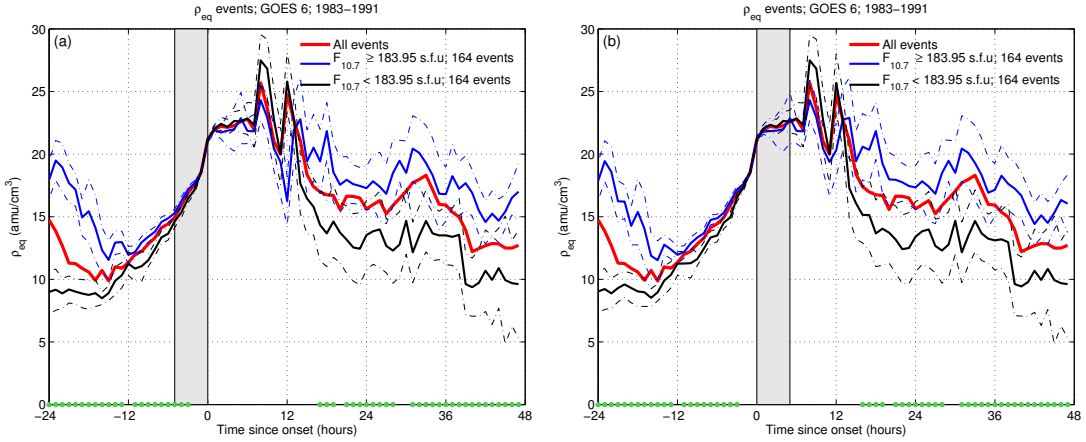

Figure 9: ρ_{eq} events of Figure 7 separated by the average $F10.7$ value (a) at onset and four hours before, and (b) at onset and four hours after.